2018

Hydrogen Isotope Separation in Metal-Organic Frameworks

Naiyuan Zhang
Oberlin College

Hydrogen Isotope Separation in Metal-Organic Frameworks

Naiyuan Zhang (James)

Mentor: Professor Stephen FitzGerald

March 30, 2018

Executive Summary

In this thesis we present our research on hydrogen isotope separation using metal-organic frameworks (MOFs). Deuterium is one of the two stable isotopes of hydrogen. Despite its wide range of application, currently there is no ideal industrial method that can separate deuterium in a fast and efficient fashion. MOFs are a class of porous materials consisting of metal ions or clusters connected by organic ligands. They have shown great potential in separating hydrogen isotopes via quantum sieving effect. In this thesis, we first provide background on two state-of-art MOFs, Co-MOF-74 and Cu(I)-MFU-4*l*. Then we elaborate on the statistical theory of selectivity, the mechanism of separation and the basic idea of mass spectrometry, which is the main analytical technique used in this project. We present temperature programmed desorption (TPD) spectra for both samples. Direct separation measurement is made with Co-MOF-74. We confirm that TPD spectra can predict the results of direct separation measurements. The TPD spectra of Cu(I)-MFU-4*l* predict a selectivity of approximately 6 at easily accessible temperatures ($\sim$260K). This shows the practicality of using Cu(I)-MFU-4*l* for hydrogen isotope separation. Preferential adsorption separation is also performed with Co-MOF-74. The extracted activation energy agrees to within 10% of literature predictions based on quantum zero point energy models.

Acknowledgements

I thank Professor Stephen FitzGerald for his mentorship through out this project.

I also thank all the fellow students in the lab.

Dedicated to my parents.

Contents

List of Figures

Chapter 1

Introduction

1.1 Motivation

Deuterium (^{2}H or D) is one of the two stable isotopes of hydrogen (the other being hydrogen-1 or hydrogen, symbol ^{1}H or H). It has a very low abundance on Earth (0.0156% by population) compared with that of the typical hydrogen (99.98% by population).[1][2] Despite the rareness, it has a large number of applications ranging from deuterated drugs to neutron moderation in nuclear reactors.[3][4][5] It also plays important roles in scientific research by serving as the tracer element in chemical reactions or the solvent in nuclear magnetic resonance spectroscopy.[6][7] Given its widespread applications, the separation of deuterium from hydrogen is of particular interest. Nonetheless, because hydrogen and deuterium are very similar to each other—the only difference being the additional neutron in the deuterium nucleus—their separation is considered to be particularly difficult: As shown in Table 1.1, no current existing separation process has all three of the

Process	Selectivity	Energy Use	Natural Exchange Rate
Distillation of H_2O	1.015 to 1.055	Very high	Moderate
Distillation of Liquid H_2	~ 1.5	Moderate	Slow
Water electrolysis	5 to 10	Very high	Fast
Laser Isotope Separation	> 20000	Moderate	Slow
Water-Hydrogen sulphide exchange	1.8 to 2.3	High	Fast
Ammonia-hydrogen exchange	2.8 to 6	Moderate	Slow-catalyst needed
Aminomethane-hydrogen exchange	3.5 to 7	Moderate	Slow-catalyst needed
Water-hydrogen	2 to 3.8	Moderate	Negligible-catalyst needed

Table 1.1: Possible industrial processes for hydrogen isotope separation with their selectivity, energy usage, and natural exhange rate. None of the processes has all three desired proprieties. Note that all the processes included here has "heavy water" (D_2O) as the final separation product whereas separation techniques using MOF has deuterium gas (D_2) as the final product.[8]

desired properties:[8]

1) high selectivity (> 5). 2) low energy usage. 3) high natural exchange rate

where selectivity is a measure of the effectiveness of the separation process (see Eqn. 2.1 and 2.2 for a more rigid definition) and natural exchange rate indicates how fast the separation proceeds.

This lack of ideal process has motivated researchers to find new techniques for hydrogen isotope separation using metal-organic frameworks (MOFs).[9] MOFs are porous compounds consisting of metal ions or clusters connected by organic ligands.[10] Studies have shown that MOFs, when used as hydrogen isotope separation techniques, have high selectivities (as high as 12 at 60K) and high natural exchange rates.[11] Although the energy usage of separation methods with MOFs

is still subject to more a comprehensive study, it is widely accepted that MOFs are promising candidates for hydrogen isotope separation techniques.[9][10][11]

1.2 Metal-Organic Frameworks

As mentioned above, MOFs are porous coordination compounds with organic ligands and metal ions. After synthesis, the pores are usually filled with so-called "guest molecules" which are bonded with metal ions.[12] In many cases, the pores are stable during the elimination of the guest molecules and could be refilled with other compounds. This elimination process sometimes causes the presence of unsaturated metal ions in MOFs. These unsaturated metal ions demonstrate the classical Coulomb attraction and hence form adsorptive sites with stronger binding energies (compared with that of regular sites, $\sim$10 kJ/mol vs. $\sim$5 kJ/mol) which are referred to as "open metal sites."[13] Since "open metal sites" have special strength in hydrogen adsorption, MOFs with these sites are of our research interest.

Another general yet valuable character of MOFs is their chemical tunability, which allows them to be synthesized in different structures by connecting different metal ions or clusters with different organic ligands. As a result, MOFs can manifest different specific areas, porosities, binding energies, and other adsorption parameters.[14] In the following, we give brief descriptions of the two MOFs examined in this project, including Co-MOF-74 and Cu(I)-MFU-4l.

1.2.1 Co-MOF-74

M-MOF-74 represents a family of isostructural MOFs, where M is a placeholder for one of six metals including manganese, iron, cobalt (Co), nickel, copper, and zinc. In this project, we focus our investigation on Co-MOF-74 and specifically the (dobdc) allotrope, where (dobdc) denotes the organic ligand 2,5-dioxido-1,4-benzenedicarboxylate. Since Co-MOF-74 (dobdc) is the only allotrope of Co-MOF-74 concerned in this project, we will refer to it simply as Co-MOF-74 in the following work.

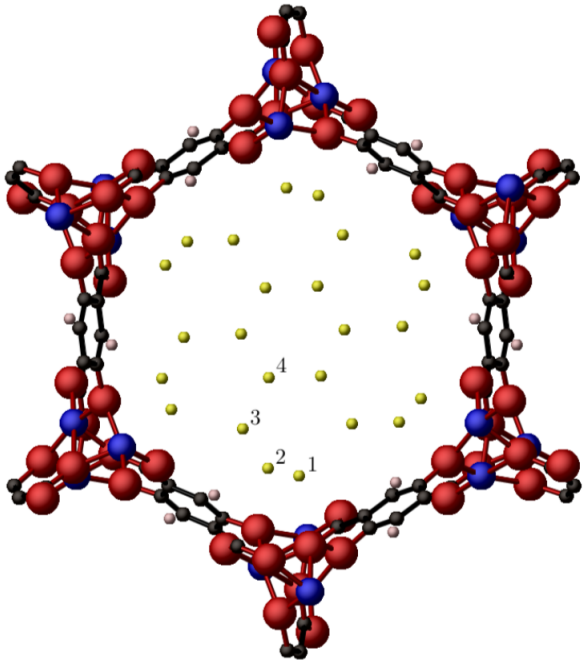

Figure 1.1: Crystal structure of Co-MOF-74[13][15][16]

Red spheres represent oxygen atoms, blue spheres represent cobalt atoms, black spheres represent carbon atoms, and light pink spheres represent hydrogen atoms. Yellow spheres in the pore represent the four adsorption sites for H2 molecules. (labeled in order of binding energy magnitude from strong to weak). Site 1 is the open metal site.

Co-MOF-74 has chemical formula:

$$Co_2(C_8H_2O_6), \tag{1.1}$$

and a molar mass of ∼312g/mol. It has an isosteric heat of adsorption 10.8 kJ/mol[16]. Fig. 1.1 shows the crystal structure of a single pore of Co-MOF-74. Both powder X-ray and neutron diffraction shows that each Co-MOF-74 has four adsorptive sites among which the strongest is the open metal site that we are interested in.[13][16]

1.2.2 Cu(I)-MFU-4*l*

Cu(I)-MFU-4*l* is a memeber of the isostructural MFU-4-type frameworks. It is constructed based on its parent cage, MFU-4*l*, through replacing some of the terminal Zn-Cl sites by Cu(I) metal sites.[17]

Cu(I)-MFU-4*l* has chemical formula:[17][18]

$$Cu_2Zn_3Cl_2(N_6H_4C_{12}O_2)_3 \tag{1.2}$$

and a molar mass of ∼1186g/mol. It has an isosteric heat of adsorption of 32 kJ/mol.[17] Fig. 1.2 (a) shows the crystal structure of a single pore of Cu(I)-MFU-4*l*. Fig. 1.2 (b) shows one of open metal sites in the pore. Since two of the Zn-Cl sites are replaced, we claim that there are two open metal sites for each Cu(I)-MFU-4*l*.[17][18].

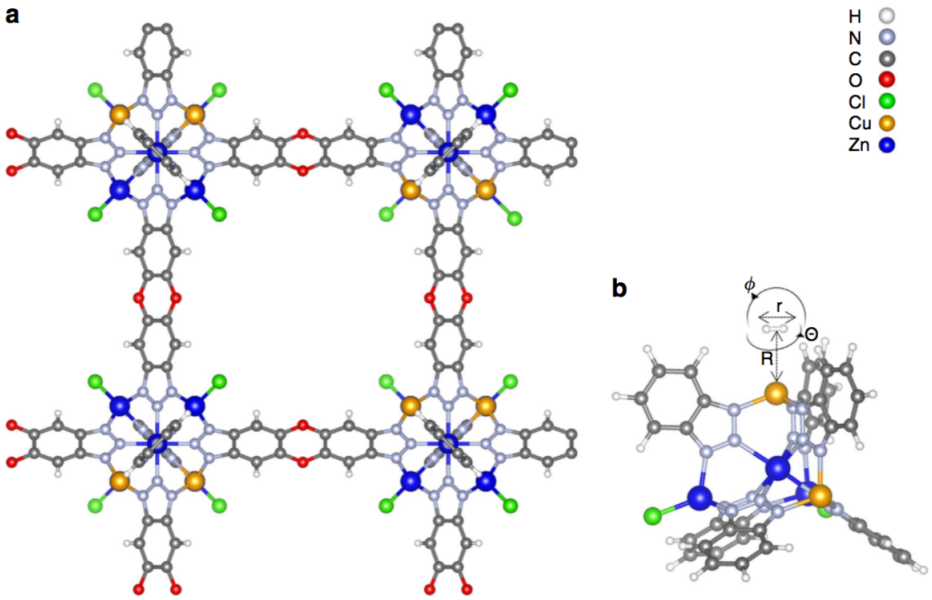

Figure 1.2: Crystal structure of Cu(I)-MFU-4*l*[17]

(a) Structure of a full pore of Cu(I)-MFU-4*l* crystal; (b) model of an open metal site of Cu(I)-MFU-4*l*. Color legend shown in the figure. R is the distance between Cu and the hydrogen centre, r is the H–H bond length of an adsorbed hydrogen; θ is the angle of rotation in the plane normal to R, and ϕ is the angle of out-of-plane rotation.

Chapter 2

Theory

2.1 Selectivity

Separation is a process through which a mixture is converted into two or more distinct product mixtures, at least one of which is enriched in one or more of the original mixture's constituents. [19] In the case of separating one isotope from other isotopes, this process can be modeled by a binary classification: Given some isotope mixture, the separation mechanism is asked to "classify" (physically separate) the mixture into two groups, with one group of the target isotope (positive) and the other group of other isotopes (negative). However, the classification process might not be perfectly done: there are mismatches between the separation and the reality. To evaluate the effectiveness of this separation, four terms are defined as the following:[20]

True positive (TP): the number of target isotope classified as target isotope

False positive (FP): the number of other isotopes classified as target isotope

False negative (FN): the number of target isotope classified as other isotopes

True negative (TN): the number of other isotopes classified as other isotopes

Selectivity (or separation factor, or diagnostic odds ratio, symbol S) is then defined as:[21][22]

$$\mathrm{S} = \frac{TP/FP}{FN/TN}. \tag{2.1}$$

To apply the same rationale to our case, consider the following example: Given some hydrogen isotope mixture, the separation process yields us two groups, denoted as "product" and "residue." The product is a mixture with higher concentration of deuterium and the residue is a mixture with higher concentration of hydrogen (both compared with the original mixture). Now the four terms are defined as the following:

True positive (TP): the number of deuterium in product

False positive (FP): the number of hydrogen in product

False negative (FN): the number of deuterium in residue

True negative (TN): the number of hydrogen in residue

And selectivity is therefore defined as:

$$\mathrm{S} = \frac{TP/FP}{FN/TN} = \frac{n_{p\mathrm{D}}/n_{p\mathrm{H}}}{n_{r\mathrm{D}}/n_{r\mathrm{H}}}, \tag{2.2}$$

where $n_{x\mathrm{Y}}$ represents the amount of Y molecules in x: p and r stand for "product" and "residue" respectively; H and D stand for hydrogen and deuterium respectively.

2.2 Quantum Sieving Effect

Quantum sieving effect (QSE) is the main mechanism for hydrogen isotope separation with MOFs under our consideration. Consider an absorptive site potential approximated with a quantum simple

harmonic oscillator. The zero point energy (the energy at lowest energy level, ZPE) of a hydrogen isotopologue gas molecule in this potential is given by:

$$E_0 = \frac{1}{2}\hbar\omega, \tag{2.3}$$

where $\hbar$ is the reduced plank constant and ω is the angular frequency which is given by:

$$\omega = \sqrt{\frac{k}{m}}, \tag{2.4}$$

where k is the characteristic spring constant and m is the mass of the gas molecule. Following Eqn. 2.3 and 2.4, clearly, the ZPE of a hydrogen isotopologue gas molecule in a quantum simple harmonic potential is inversely proportional to the square root of the mass of the molecule. Due the additional neutron in the nuclei, the mass of a deuterium gas molecule is two times that of the mass of a regular hydrogen gas molecule; therefore, the ZPE of a deuterium gas molecule is $\sqrt{\frac{1}{2}} = 0.71$ times that of a regular hydrogen gas molecule. While the relative difference between the ZPEs of the two isotopologues remains constant (1-0.71=0.29), the absolute difference can be increased by increasing the characteristic spring constant ($E_0 \propto \sqrt{k}$).

In Fig. 2.1, a more realistic approximation is made with a typical inter-molecule potential, Lennard-Jones potential, which is given by:

$$V_{LJ} = \epsilon\left[\left(\frac{r_m}{r}\right)^{12} - 2\left(\frac{r_m}{r}\right)^{6}\right], \tag{2.5}$$

where r represents the distance between the site and the center of mass of the adsorbate molecule, $-\epsilon$ is the minimum of the given potential, and r_m is the distance corresponding to that minimum. Similarly, by changing the parameters of the potential (ϵ and r_m in this case), the absolute difference between the ZPEs of the two isotopologues also changes.

This difference between the ZPEs leads to a difference in the binding energies for the two

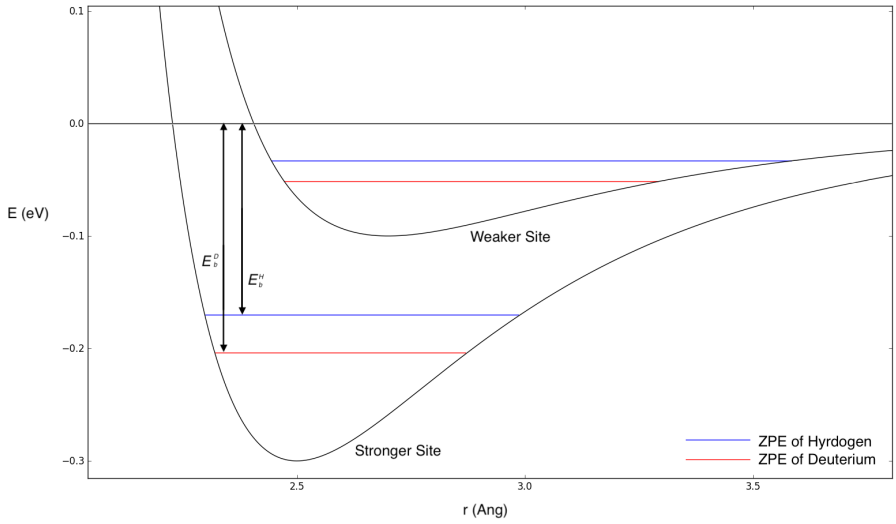

Figure 2.1: A qualitative example of ZPEs in different potentials

Each of the black curves represents the potential from an adsorptive site of a MOF: the one above is for Co-MOF-74, whereas the one below is for MFU. E_b^{H} and E_b^{D} indicate the binding energies that gas molecules experience in MOFs.

isotopologues (as indicated in Fig. 2.1). Since D_2 molecules experience a higher binding energy than H_2, they are more preferentially adsorbed onto the adsorption sites of the MOF sample. In another sense, if both molecules (H_2 and D_2) are adsorbed, D_2 will need a higher kinetic energy to escape from the adsorptive site. These two ways of understanding naturally lead to two separation methods, which are referred to as preferential adsorption separation and temperature-programmed separation. [15]

2.2.1 Preferential Adsorption Separation

Preferential adsorption separation (PAS) is a separation process in which deuterium molecules are preferentially adsorbed in to the open metal site. As shown in Fig. 2.2, a 1:1 mixture of hydrogen and deuterium is exposed to the MOF sample at a relatively low temperature (77K in this example). After the system has reached the equilibrium, some of the mixture is adsorbed in the MOF whereas the rest remains in the gas phase. Because deuterium are energetically more favorable to be adsorbed, there are more deuterium molecules than hydrogen molecules in the MOF whereas there are more hydrogen molecules in the remaining gas mixture.

After evacuating the remained gas mixture (which can be cycled to another round of separation), the adsorbed mixture is released and obtained as the separation product by heating up the system. Based on the definition in Eqn. 2.2, selectivity for this separation mechanism has the following form:

$$\mathrm{S} = \frac{n_{a\mathrm{D}}/n_{a\mathrm{H}}}{n_{g\mathrm{D}}/n_{g\mathrm{H}}}, \tag{2.6}$$

where a and g stand for "adsorbed" and "gaseous" correspondingly.

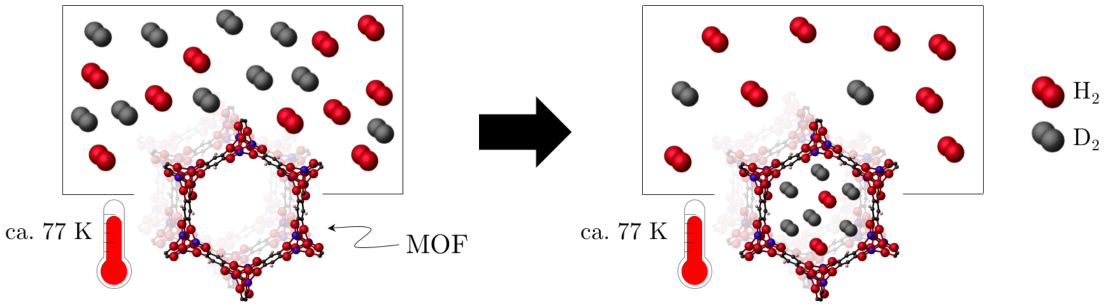

Figure 2.2: A scheme of preferential adsorption separation.[15]

2.2.2 Temperature-Programmed Separation

At the beginning of a temperature-programmed separation (TPS), a 1:1 mixture of hydrogen and deuterium is exposed to the MOF sample. The temperature of the system is decreased to a low enough value so that nearly all the gas molecules are adsorbed onto the MOF ($\sim$ 10K). Then, as shown in Fig. 2.3, the system is heated to a higher temperature (77K in this example). Because deuterium molecules require higher kinetic energy to escape from the site, they are less likely to be desorbed than hydrogen molecules at the same temperature. Hence the desorbed gas mixture has more hydrogen than deuterium, whereas the remained adsorbed mixture has more deuterium than hydrogen.

Similarly, after evacuating the desorbed gas mixture (which can be cycled to another round of separation), the adsorbed mixture is released and obtained as the separation product by heating up the system. Selectivity for this mechanism also has the form of Eqn. 2.6. Note that "gas phase" in the equation refers to the desorbed mixture in this case.

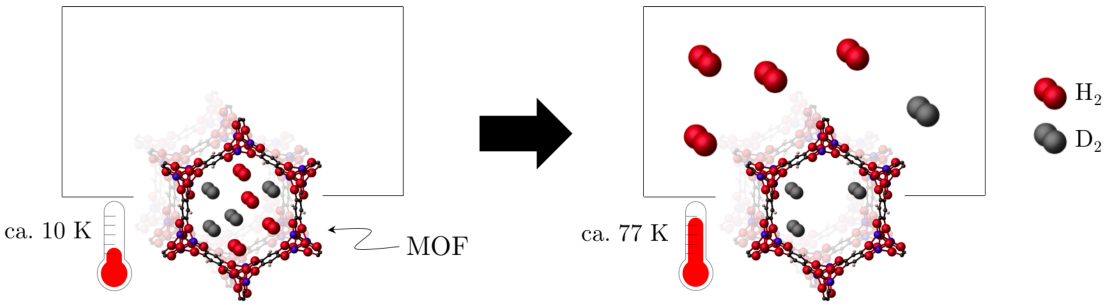

Figure 2.3: A scheme of temperature-programmed separation.[15]

2.3 Mass Spectrometry

Mass spectrometry is the main analytical technique used in this project. It is utilized to quantitatively examine the components of the gas mixtures. In this section, we will briefly explain the mechanisms and characters of a general mass spectrometry (and mass spectrometer). Details that are related to the specific mass spectrometer we used will be discussed in Chapter 3 Section 3.

A mass spectrometer is an apparatus to perform a mass spectrometry. It has three components, including an ionizer, a mass analyzer, and a detector. The ionizer ionizes a portion of the input sample. The mass analyzer sorts the ions (ionized sample molecules) by their mass-to-charge ratios. The detector measures the the relative abundance of different ions. A theoretical example is depicted in Fig. 2.4

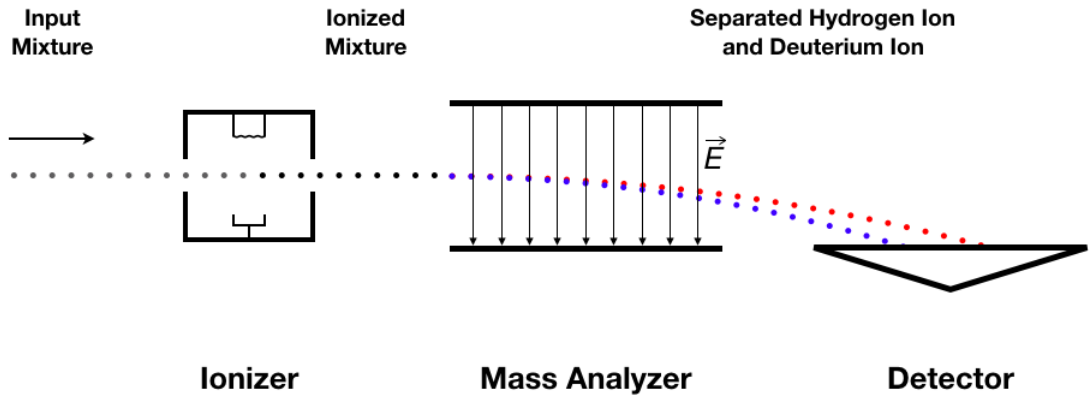

Figure 2.4: A theoretical example of mass spectrometry.

The separated hydrogen ions (H_2^+) and deuterium ions (D_2^+) are represented in blue and red dots correspondingly

As shown in Fig. 2.4, the input hydrogen and deuterium gas mixture (grey dots) flows into

the ionizer and become ionized. Depending on the type of the ionizer, the molecules can be either positively or negatively charged; we assume that they are positively charged by e in this example. The ionized mixture (black dots) then flows into the mass analyzer. A mass analyzer can use either electric field or magnetic field or both, but in any case, the guiding principle is the Lorentz force law and Newton's second law:

$$\vec{F} = Q(\vec{E} + \vec{v} \times \vec{B}), \tag{2.7}$$

$$\vec{F} = m\vec{a}. \tag{2.8}$$

Combining these two equations yields us a differential equation:

$$\left(\frac{m}{Q}\right)\vec{a} = \vec{E} + \vec{v} \times \vec{B} \tag{2.9}$$

In our example, the mass analyzer only uses an electric field $\vec{E}$. Also, since the hydrogen and deuterium gas mixtures are both positively charged by e, Eqn. 2.9 therefore yields:

$$\left(\frac{m_{\mathrm{H}}}{e}\right)\vec{a_{\mathrm{H}}} = \vec{E} = \left(\frac{m_{\mathrm{D}}}{e}\right)\vec{a_{\mathrm{D}}}, \tag{2.10}$$

where m_{H} and m_{D} are the masses of hydrogen and deuterium gas molecule. Since $m_{\mathrm{D}} = 2m_{\mathrm{H}}$, we have $\vec{a}_{\mathrm{H}} = 2\vec{a}_{\mathrm{D}}$, which means the heavier deuterium ions are deflected less than the lighter hydrogen ions. Therefore, deuterium ions (red dots) hit onto the detector at a further position compared with hydrogen ions (blue dots). Finally, the detector records the number of "hits" at different position and obtains the information to calculate the relative abundance of hydrogen and deuterium molecules in the original input mixture.

Chapter 3

Experimental Apparatus

3.1 Loading and Mixture Preparation System

We use a Micromeritics Accelerated Surface Area and Porosimetry System model 2020 (ASAP 2020) and an additional 150cm^3 volume as our loading and mixture preparation system. As shown in Fig. 3.1, the two loading volumes are V40 and V150. Valves P1 and P2 connect V40 to the same pump through tubes with different diameters, which allow us to pump on the rest of the system with different rates. The pressure gauge set includes one gauge with lower range but higher precision (up to ∼12mbar, ±0.0001mbar) and another gauge with higher range but lower precision (up to ∼1200mbar, ±0.01mbar). All the valves that are built-in inside the ASAP 2020 are controlled through the software ASAP 2020 V4.01.01 on a PC.

When loading gas, the main assumption is that H_2 and D_2 behave as ideal gases. And

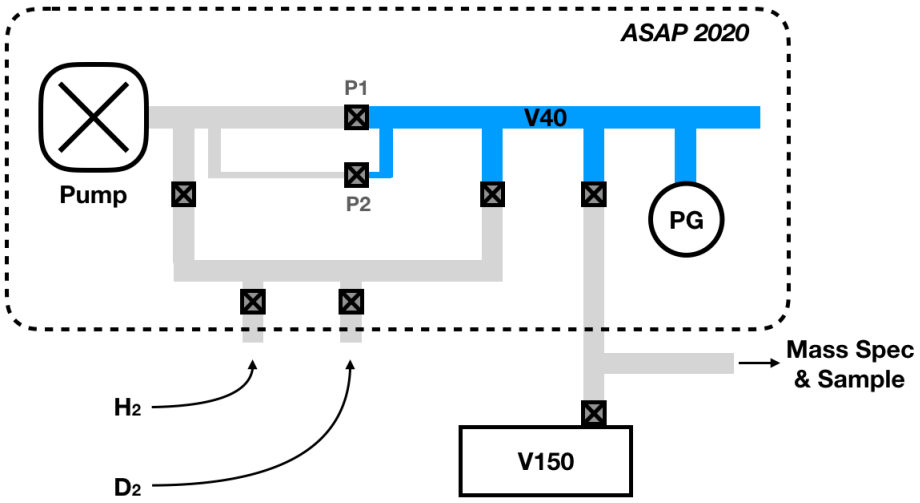

Figure 3.1: A diagram of the loading and mixture preparation system. Everything contained in the dashed rectangle is built-in inside the ASAP 2020. V40, indicated with blue, is a 40cm^3 volume; V150, shown as the solid rectangle, is a 150cm^3. PG represents a set of pressure gauges. Each of the two valves on the bottom left connects to a high pressure cylinder containing pure H_2 or D_2 (as indicated in the figure). The tube on the right connects to the mass spectrometer and the sample.

therefore obey the ideal gas law:

$$PV = nRT, \tag{3.1}$$

where P is loading pressure, V is loading volume, n is the amount of gas molecules, R is the gas constant, and T is absolute temperature of the loading volume. Straightforwardly, the amount of gas loaded is given by

$$n = \frac{PV}{RT}. \tag{3.2}$$

3.2 Sample Environment

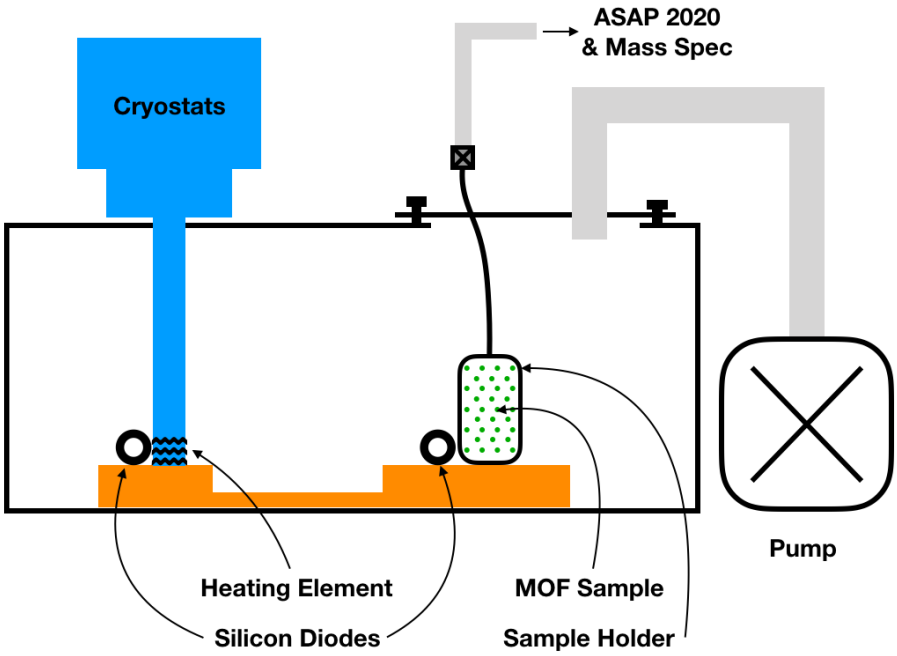

Figure 3.2: A diagram of the sample environment.

The solid black rectangle represents the high vacuum chamber. The copper sample mount is indicated in orange. The solid black curve below the valve represents a thinner tube that connects to the sampler holder. (LakeShore TC and Sumitomo compressor not shown)

As shown in Fig. 3.2, the sample environment is created inside a high vacuum chamber ($< 10^{-5}$ mbar). This high vacuum chamber thermally isolates the sample from the hot air in the room (∼298K) and allows us to cool the sample with a cryostat cold finger. Here, we use a Janis ST-300T compact cryostats supported by a HC-4E indoor water-cooled compressor from Sumitomo. A small resistor is placed around the cold finger as a heating element. Two silicon diodes are used

to measure the temperature inside the vacuum chamber: one is placed near the sample whereas the other is placed directly under the cold finger. The heating element and two diodes are all connected to a LakeShore 331 temperature controller (TC). This entire system allows us to have a control over the environment (temperature-wise) of the sample over a range from 12K to 290K.

As a side note, the entire high vacuum chamber is placed inside a Bomem DA3 infrared spectrometer. The high vacuum is created by a Alcatel Adixen 2015 SD Pascal dual stage rotary vane vacuum pump.

3.3 Mass Spectrometer

The mass spectrometer we use is a triple filter quadrupole mass spectrometer from Hiden 3F Series. Because the gas sample can very possibly have a higher pressure than the operating pressure of the mass spectrometer, the sample inlet system is built with a thin capillary that serves as a pressure-reducing mechanism.[23] The ionizer bombards the sample molecules with energetic electrons (70 eV) and ionizes them into positive ions.[23] This process is described as:[24]

$$M + e^- \longrightarrow M^+ + 2e^-, \tag{3.3}$$

where M represents the molecule sample being ionized, e^- represents a electron and M^+ represents the resulting ion.

The triple filter quadrupole mass analyzer consists of three quadrupole mass filters. Each quadrupole filter consists of four parallel metal rods. Each opposing rod pair is electrically connected. A radio frequency AC voltage is applied to one of the two pairs whereas a DC offset voltage is applied to the other pair.[23] The electric field created by the voltages accelerates the sample

ions differently based on their mass-to-charge ratios (as shown in Eqn. 2.9); only ions with certain ratios can pass through the quadrupole and reach the detector. The arrangement of three linearly aligned quadrupole mass filters is designed to enhance the quantitative performance of the mass analyzer.[25]

There are two detectors in our mass spectrometer, including a Faraday cup and a secondary electron multiplier (SEM). The advantage of a SEM detector is that it amplifies the signal from the ionized samples and therefore has a higher sensitivity compared with a Faraday cup detector.[26][27] This higher sensitivity makes SEM particularly suitable for low pressure sample detecting (order of magnitude of 10^{-1}mbar in our case) and therefore is primarily used in this project.

3.3.1 Relative Sensitivity Factor

A given mass spectrometer responses to different gas molecules with different sensitivities. For instance, when given an arbitrary amount of 1:1 mixture of gaseous hydrogen and deuterium, our mass spectrometer measures the mixture to be roughly 3:1 in ratio because it is more sensitive to hydrogen than to deuterium. Straightforwardly, we define the relative sensitivity factor (RSF) of hydrogen to be 3 relative to deuterium. As a measure of instrumental sensitivity, RSF depends on a variety of sensitivity factors originated from different components of the mass spectrometer and is expressed as: [23]

$$\mathrm{RSF} = \mathrm{R_I} \cdot \mathrm{R_S} \cdot \mathrm{R_F} \cdot \mathrm{R_Q} \cdot \mathrm{R_D}, \tag{3.4}$$

where RSF is the overall relative sensitivity, $\mathrm{R_I}$ is the inlet sensitivity factor, $\mathrm{R_S}$ is the source sensitivity factor, $\mathrm{R_F}$ is the fragmentation factor, $\mathrm{R_Q}$ is the quadrupole transmission, and $\mathrm{R_D}$ is the detection efficiency.

When the inlet system reduces the pressure of the sample gas, it only allows a fraction of the sample passes through the capillary. However this fraction is different for different type of gases. Hence fractionation in the inlet system contributes a sensitivity factor R_I.

The ionizer contributes two factors including R_S and R_F. Since the ionizer only ionizes a portion of the sample molecules, the size of the portion varies from gas to gas and is described by R_S. During the ionization process, sample might break into smaller fragment ions and change its mass-to-charge ratio. For example when a hydrogen molecule is ionized, the expected resulting ion is H_2^+, which has a mass-to-charge ratio of 2 amu/e. But the fragmentation might cause the resulting ions to be 2 H^+ ions which each has a mass-to-charge ratio of 1 amu/e. Because a mass spectrometer distinguishes samples by their mass-to-charge ratios, the H^+ ions will not be counted as hydrogen when they hit the detector hence creating a signal loss. The fragmentation rate also varies from gas to gas and is described with R_F.

R_Q originates from the mass analyzer. This is not a very significant factor in our case since it is effectively a constant for hydrogen and deuterium. Although it is reported that for a quadrupole mass analyzer, the transmission tends to reduce at higher masses. R_D is related to the nature of the type of the detector. The efficiency of a Faraday cup is a constant for all masses whereas the efficiency of SEM detector is inversely proportional to mass. [23]

Note that RSF is traditionally defined relative to nitrogen.[23] But since hydrogen and deuterium are the only two gases concerned in this project, we arbitrarily define RSF of deuterium to be 1. And as suggested by the manufacturer, experimental measurements on RSF of hydrogen is performed. Similar to the description in the beginning of this subsection, an arbitrary amount of 1:1 mixture of gaseous hydrogen and deuterium in sampled by our mass spectrometer. This yields

a RSF for hydrogen of 2.81±0.002 (relative to deuterium).

It is important to note that, RSF changes significantly if the measurements of hydrogen and deuterium are done separately: Instead of feeding a 1:1 mixture of hydrogen and deuterium, we first feed some amount of pure hydrogen, then vacuum the system and feed the same amount of pure deuterium. Based on the previous result, we expect the mass spectrometer to report 2.81 times more hydrgoen than dueterium. However, this experiment yields a different RSF=3.58±0.06 for hydrogen relative to deuterium. Even though we don't have a comprehensive explanation to this interesting discrepancy, the difference in experimental procedures seems to imply a concentration-dependent RSF. But without further investigation, we for now naively decide that RSF in our mass spectrometer has a value of 2.81±0.002 for any hydrogen-deuterium mixture and a value of 3.58±0.06 for pure hydrogen versus pure deuterium.

3.4 Overall Setup

Fig. 3.3 is a diagram of the overall experimental apparatus setup. As shown in the figure, the diodes and the heating element are connected to the TC for temperature controlling. A National Insturments Terminal Block is introduced as a computer interface allowing further data collection by a PC. The mass spectrometer directly send data signals to the PC through an ethernet cable. Mass spectrometry, pressure, and temperature data are collected via the software MASoft 7 Professional. Pressure and temperature data are also monitored by a LabView program. The adjustable valve allows us to tune the effective diameter of the tube which further allows us to control the pumping rate (similar to P1 and P2 in Fig. 3.1).

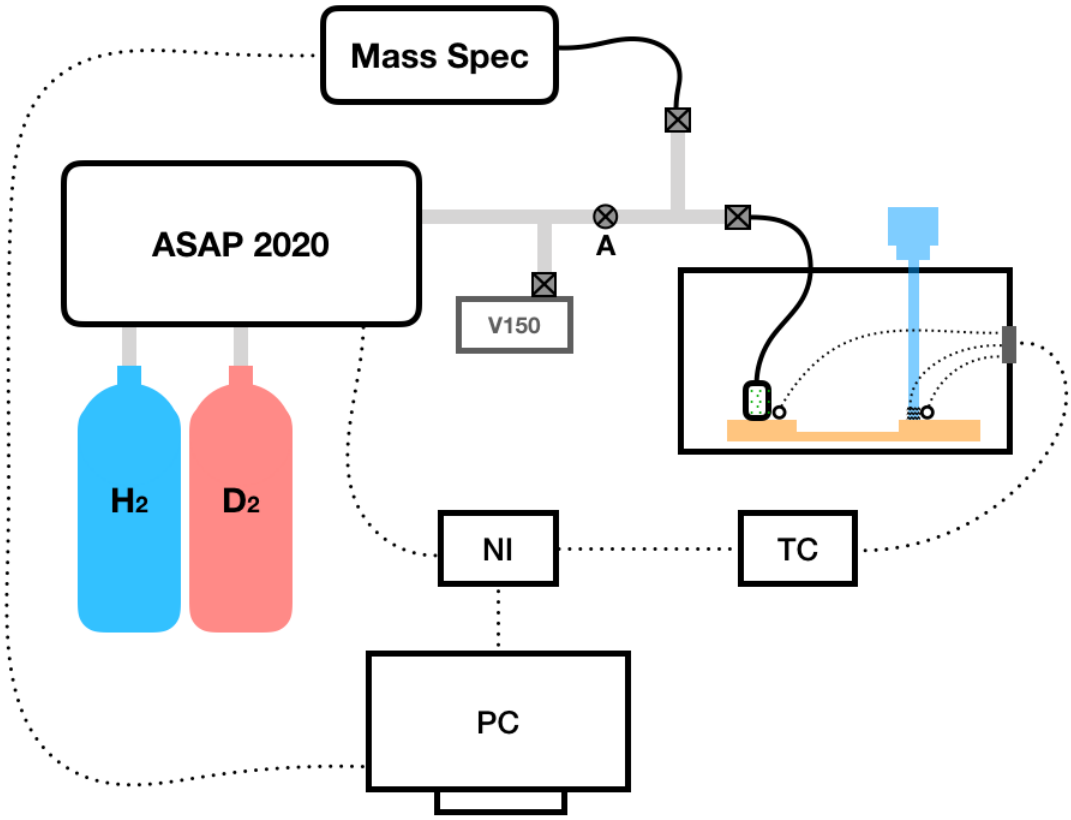

Figure 3.3: A diagram of the overall setup.

Solid curves represent thinner tube or capillary, dotted curves represent electrical wires, TC represents the LackShore TC, and NI represents a National Instruments computer interface. The circle-shaped valve, denoted with A in the figure, is a adjustable valve.

Chapter 4

Experimental Procedure

4.1 Temperature Programmed Desorption

Temperature programmed desorption (TPD), also referred as thermal desorption spectroscopy, is a technique for probing surface desorption kinetics. In our project, we use it primarily to find the temperatures at which different hydrogen isotopes desorb from the sites in the MOFs. The TPD procedure is straightforward: First we prepare the gas sample and exposed it to the MOF under investigation. Then we decrease the temperature to a low enough value ($\sim$ 10K) to reach a complete adsorption (nearly all gas molecules are adsorbed onto the MOF). Finally, we gradually increase the temperature (5K/min) to a high enough value so that all the adsorbed molecules are desorbed ($\sim$200K for Co-MOF-74 and $\sim$290K for Cu(I)-MFU-4l) from the MOF.

We know from Langmuir isotherm equation, for a given temperature, the fraction of site

occupation of a solid is related to the pressure around the solid. Therefore the increasing pressure in the system caused by gas desorption will in turn cause the desorbed molecules to re-adsorb. To aviod this re-adsorption, we keep vacuuming the system during the heating process. The desorption rate of the gas sample is then monitored using the mass spectrometer as a function of temperature.

4.2 Temperature Programmed Separation

The procedure of a TPS is very similar to the procedure of a TPD. The only difference is in the heating process. Instead of heating the sample to a high enough value so that all the adsorbed molecules are desorbed, we only heat the sample to a relatively high temperature (e.g 77K) so that only a portion of the gas sample desorbs from the MOF. This relatively high temperature is denoted as T_{close}. Similarly, to avoid re-adsorption, we keep pumping on system during the heating process. Now that the original gas sample is physically isolated into two portions, one being gaseous (evacuated) and the other being adsorbed, the separation is completed.

As discussed in section 2.2, this separation will make deuterium concentrate in the adsorbed portion. Since deuterium is our target isotope, we denote the adsorbed portion as the product of this separation and the evacuated gaseous portion as the residue. Now to evaluate this separation, we stop vacuuming the system and heat the sample to a high enough temperature so that the product is desorbed. The components of the desorbed product are then measured with the mass spectrometer.

4.3 Preferential Adsorption Separation

The procedure of PAS is the following: First we cool the MOF to a relatively low temperature (e.g. 77K), denoted as T_{ads}. Then we prepare the gas sample and expose it to the MOF for a long time (∼8h). After the system has reached equilibrium, a portion of the original sample is adsorbed onto the MOF and the remaining portion is still in gas phase. Now that the original gas sample is physically isolated into two portions, the separation is completed.

The evaluation process is very similar to that of the TPS: We define the adsorbed portion as the product and the gaseous portion as the residue. The component of the residue is measured with the mass spectrometer first. Then we evacuate the residue and heat the sample to release the product. The component of the product is then measured with the mass spectrometer.

4.4 Miscellaneous Notes

There are several details to pay attention to when performing the above-mentioned experiments. Here I provide a list of the details that I have noticed.

When a mixture is made during the gas sample preparation, it requires some long period of time to reach equilibrium. We experimentally tested the time required for hydrogen and deuterium to mix in our system. The measurement yields a minimum time of 5h. Since the unevenness of the mixture might have unpredictable effects to the adsorption process (for a exaggerated example, consider the case in which only hydrogen molecules reach the MOF and get adsorbed), to achieve a more informative result, it is beneficial to allow the gases to mix for a long period of time (several

hours) before exposing it to the MOF.

It is generally hard to suddenly stop heating at some given temperature for many reasons (e.g. the time lag between the controlled temperature measured from the diode under the cold finger and the sample temperature). Therefore, when performing a TPS, we in fact heat the sample gradually (5K/min) to a temperature high enough so that all the original gas sample are desorbed just as a regular TPD. To achieve the separation purpose, we close the sample valve (the valve right above the sample holder) at the desired relatively high temperature T_{close}. By doing so, the original gas sample is isolated into two portions including one above the sample valve (evacuated) and one below the sample valve. And this is why this characteristic temperature of TPS is denoted as T_{close}. Note that all the product is below the sample valve. Then the evaluation process is done as described in section 4.2.

Again by Langmuir isotherm equation, the fraction of site occupation is related to the pressure. Therefore we can force the molecules adsorbed on the MOF to desorb by pumping on the sample with a vacuum. This will cause some problems for the evaluation process for PAS. Because to avoid additional desorption of the product, we want to evacuate the residue when the sample valve is closed. But by doing so, we are leaving a portion of the residue in the sample holder and hence diluting the product. This problem can be resolved by a small correction using the pressure of each portion (above the sample valve and below). For further details on this correction, see Appendix B.

Chapter 5

Results and Analysis

5.1 Data Processing

Before any discussion on the results, we present some data processing methods that are commonly used in this project. Unless otherwise mentioned, all of the raw data from the mass spectrometry are treated with the following processes.

5.1.1 Background Calibration

Mass spectrometry data for hydrogen usually has extremely high background due to the residual water vapor (as high as 300% of the raw signal). Therefore, using a suitable method to handle the background is fundamental to the rest of the analysis. We can perform a calibration by taking background data when there is no actual hydrogen signal. As shown in Fig. 5.1 (a) a raw TPD

data for hydrogen has a very high background; the background data is circled in black. Remove the data with real hydrogen signal, and then fit the background into a curve (usually a straight line) that makes $\bar{\chi}^2$ as close to 1 as possible. This fit provides a expected background for all points in the raw data. Then subtract this expected background from the raw data. As shown in Fig 5.1 (d), the resulting curve is calibrated to have a baseline as around zero; the background is now removed.

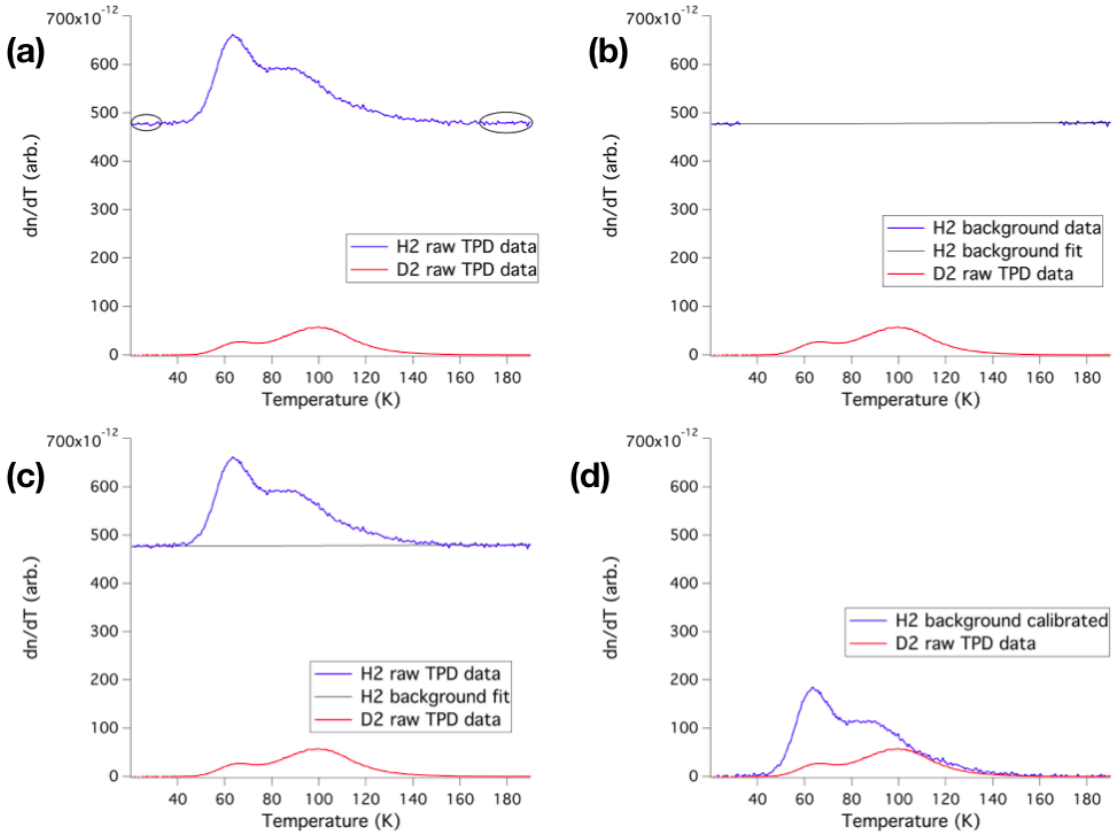

Figure 5.1: An example of background calibration.

(a) the raw data and the background data circled in black; (b) the fitting of the background; (c) the expected background for the raw data; (d) calibration completed.

5.1.2 Scaling and Smoothing

As explained in section 3.3, the mass spectrometer has higher sensitivity to hydrogen than to deuterium. Therefore the real signal is obtained via scaling down the hydrogen data by the RSF (of hydrogen relative to deuterium). Fig. 5.2 shows an example of this process.

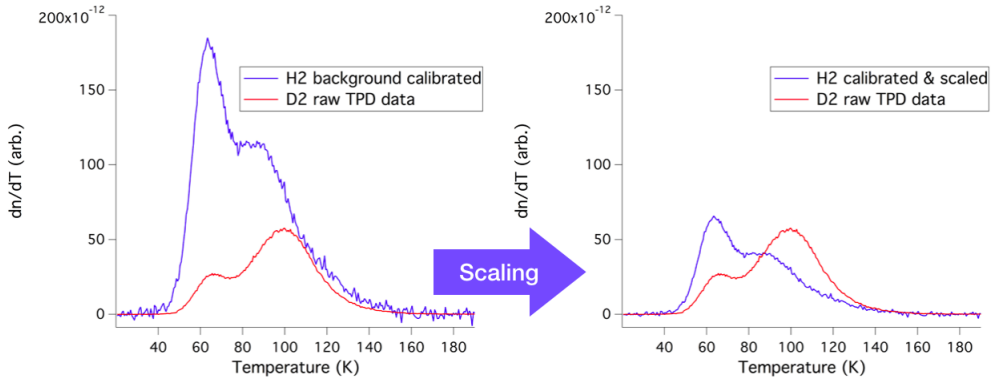

Figure 5.2: An example of scaling.

The plot that is being scaled is the equivalent of Fig. 5.1 (d), with a different plotting range.

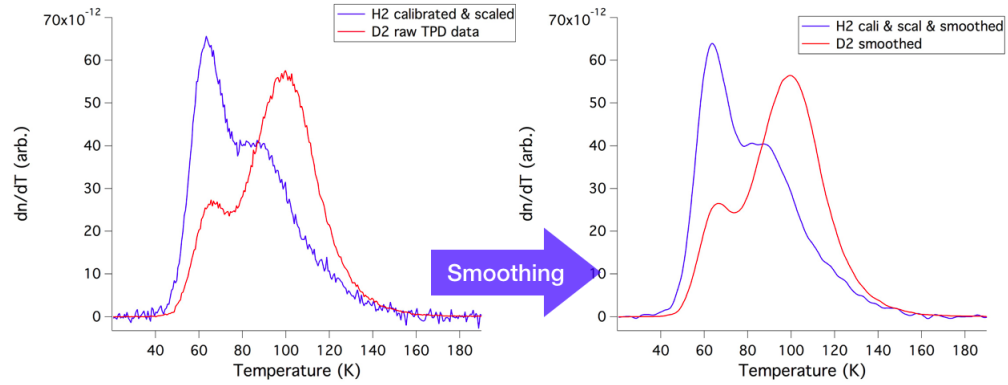

Figure 5.3: An example of smoothing.

The plot that is being smoothed is the equivalent of Fig. 5.2 (right), with a different plotting range.

Also mentioned in section 3.3, SEM detector has a higher sensitivity because it amplifies the signal. However, it also amplifies the noise. This issue can be resolved by using the smoothing function in Igor Pro. A typical smoothing factor we use is 10. Fig. 5.3 shows an example of this process.

5.2 Temperature Programmed Desorption

TPD spectra for Co-MOF-74 and Cu(I)-MFU-4*l* are obtained. As shown in Fig. 5.4 and Fig. 5.5, the desorption temperature difference between hydrogen and deuterium is 5.6K for the open metal sites in Co-MOF-74 and ∼10.6K for the open metal sites in Cu(I)-MFU-4*l*.

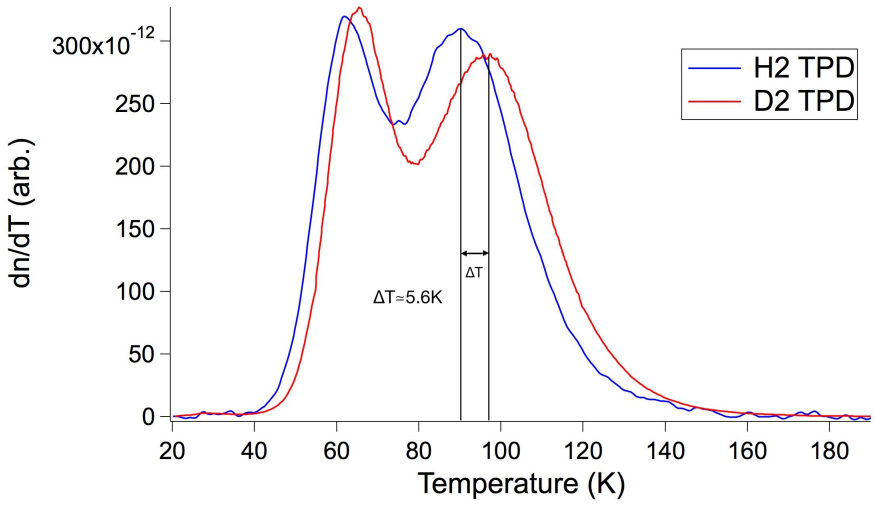

Figure 5.4: Pure-pure TPD spectra for Co-MOF-74

The peak at highest temperature corresponds to the molecules desorbed from the open metal site. The desorption of hydrogen from the open metal site peaks at ∼90.0K. The desorption of deuterium from the open metal site peaks at ∼95.6K. The difference between the desorption temperatures of hydrogen and deuterium is ∼ 5.6K.

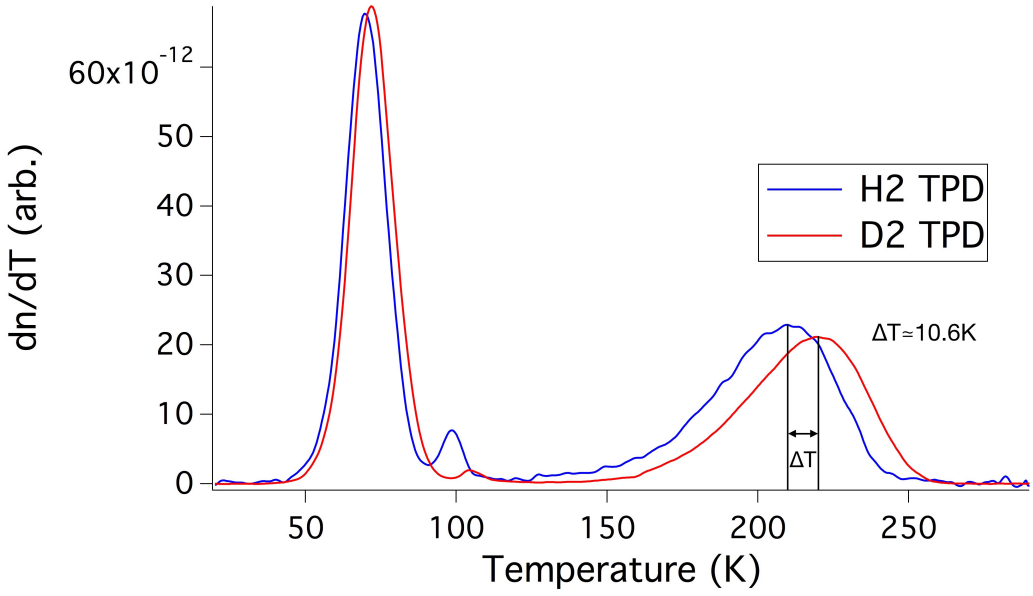

Figure 5.5: Pure-pure TPD spectra for Cu(I)-MFU-4*l*

The peak at highest temperature corresponds to the molecules desorbed from the open metal site. The desorption of hydrogen from the open metal site peaks at ∼209.2K. The desorption of deuterium from the open metal site peaks at ∼219.8K. The difference between the desorption temperatures of hydrogen and deuterium is ∼10.6K.

For each MOF, we obtained two different TPD spectra: One is a combined plot of the TPD spectrum of pure hydrogen and the TPD spectrum of pure deuterium. The other is the direct result from the TPD experiment of a 1:1 mixture of hydrogen and deuterium. The former one (presented above), denoted as pure-pure TPD spectrum, more accurately reflects how the difference between binding energies affects the difference between desorption temperatures of the gases. This is because pure gas adsorption directly relates the binding energy to the required escaping kinetic energy and further relates it to the temperature of the molecules whereas mixture gas adsorption

might have adsorbent-adsorbent interactions that influences the desorption temperatures of the gases. The later one (presented below), denoted as mixture TPD spectrum, has an application in predicting the ratio between deuterium and hydrogen in the product of a TPS. A more detailed relation between a mixture TPD and TPS will be discussed in the next section.

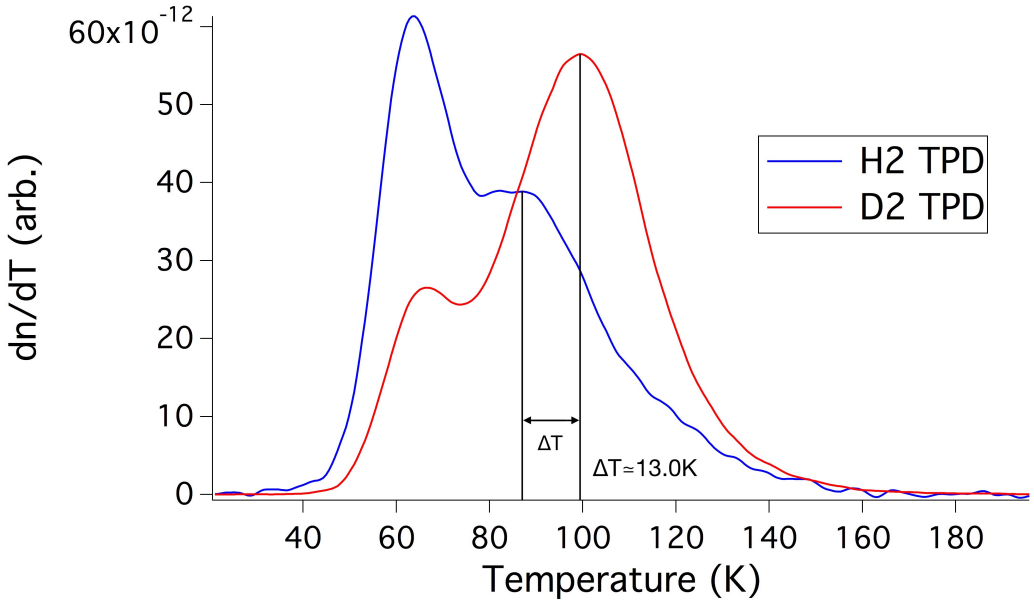

Figure 5.6: Mixture TPD spectra for Co-MOF-74

The desorption of hydrogen from the open metal site now peaks at ∼86.8K. The desorption of deuterium from the open metal site now peaks at ∼99.8K. As shown in the figure, the difference between the desorption temperatures of hydrogen and deuterium is changed to ∼13.0K.

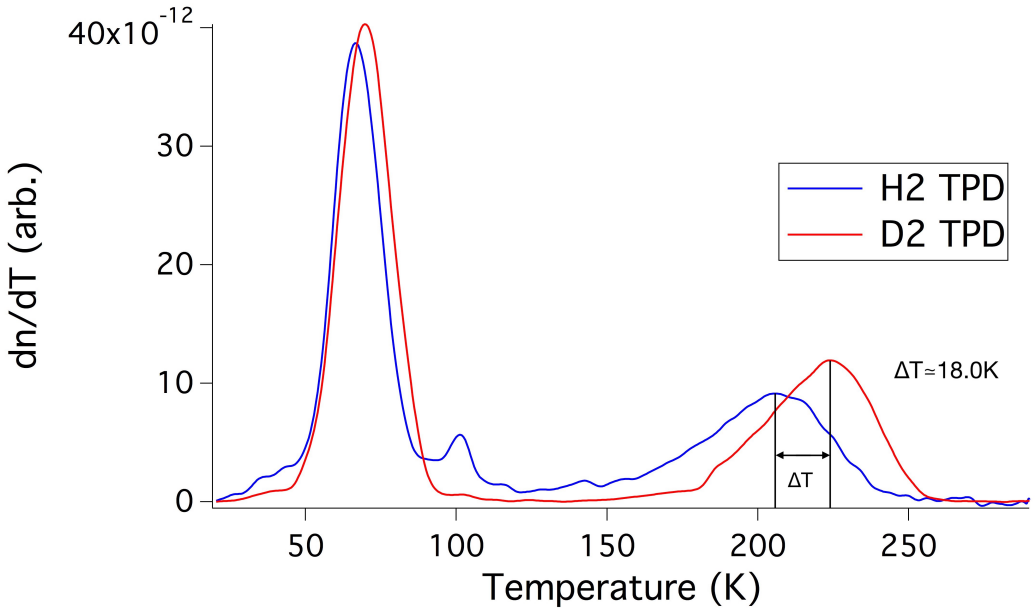

Figure 5.7: Mixture TPD spectra for Cu(I)-MFU-4*l*

The desorption of hydrogen from the open metal site now peaks at ∼205.8K. The desorption of deuterium from the open metal site now peaks at ∼223.8K. As shown in the figure, the difference between the desorption temperatures of hydrogen and deuterium is changed to ∼18.0K.

5.3 Temperature Programmed Separation

Because a mixture TPD and TPS has very similar procedures, the data from a mixture TPD can be used to predict the result of a TPS with given T_{close}. We integrate the mixture TPD spectra for Co-MOF-74 over temperature, resulting a curve of the amount of desorbed molecules against temperature as shown in Fig. 5.8 (a). Note that because at 200K, all the adsorbed molecules have been desorbed from Co-MOF-74, the value at the end of each curve (same for hydrogen and deuterium because the original mixture is 1:1) is the amount of that molecule loaded initially, temporarily denoted as x. We then find the curve of the amount of remaining molecules against temperature by subtracting the desorbed curve from x (as shown in Fig. 5.8 (b)).

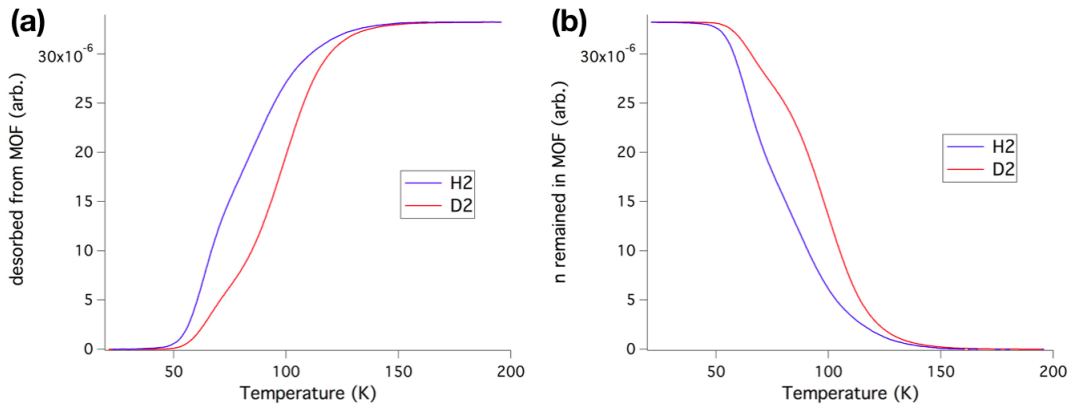

Figure 5.8: Integration of mixture TPD spectra for Co-MOF-74

(a) the amount of desorbed molecules against temperature; (b) the amount of remaining molecules against temperature

From the Fig. 5.8 (b), we find the ratio of deuterium over hydrogen remained in Co-

MOF-74 as a function of temperature as shown in Fig 5.9 black curve. Since the product of a TPS is essentially the remaining adsorbed gas mixtures when we stopped heating at the desired temperature, this black curve predicts the ratio of deuterium over hydrogen of the product of a TPS with a given T_{close}.

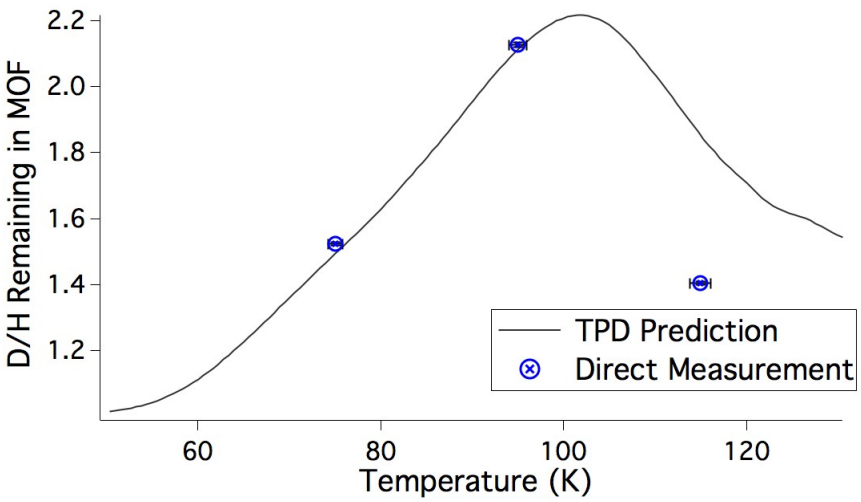

Figure 5.9: TPD predictions and direct measurements of TPS with Co-MOF-74

Note that the amount of gas are very close to each other at temperatures <50K and >130K, therefore the ratio of deuterium over hydrogen fluctuates significantly due the large relative error and hence cannot serve as a good prediction.

We then performed three TPS with a T_{close} of 75K, 95K and 115K. The products of the three separation have the ratio of deuterium over hydrogen to be 1.52, 2.13, and 1.41 separately. The TPD prediction on these three temperatures yields a result of 1.49, 2.12, and 1.83 separately. It is clear from the figure that the first two direct experimental results are very close to the theoretical predictions (within 2 standard deviations). However the last experimental result is far from the prediction with an error greater than 10 standard deviations. A possible explanation to this large

error is the following: as described in the caption of Fig. 5.9, the the ratio of deuterium over hydrogen fluctuates significantly due the large relative error at temperatures <50K and >130K. But this cut off (50K and 130K) is merely based on author's observation and does not have a solid justification (which would require a more advanced error analysis to the prediction). Therefore, it might be the case that the relative error is already large enough to cause a 20% deviation on the prediction from the experimental result at 115K, but not enough to cause obvious sudden changes (highly fluctuating). In other words, without further error analysis, we might have overly estimated the range of reasonable prediction made with this TPD prediction curve.

TPD prediction is made for Cu(I)-MFU-4*l* in the same fashion as shown in Fig. 5.10. We do not have the sufficient time to perform TPS experiments for this sample, but based on the prediction we report a highest product ratio slightly lower than 6 at $T_{close} = 263K$.

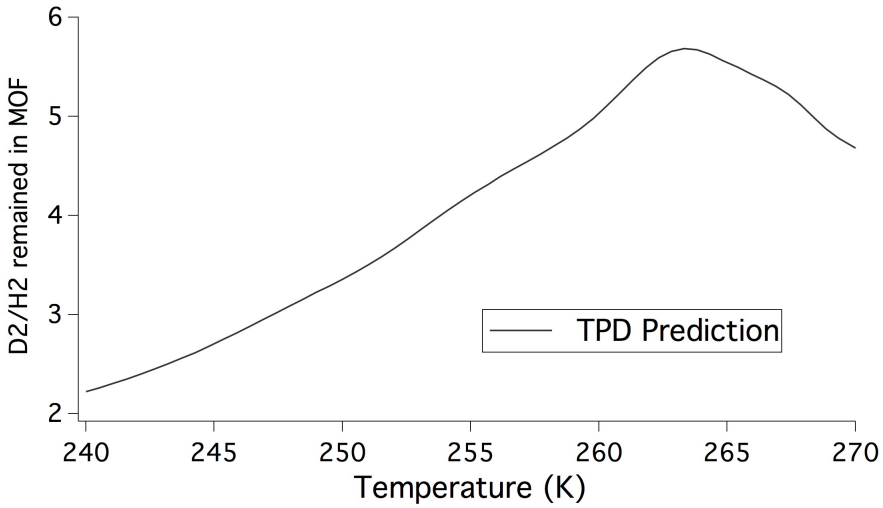

Figure 5.10: TPD predictions of TPS with Cu(I)-MFU-4*l*

Note that for this curve, the naive cutoff made by pure observation is from 150K to 270K, however here we present a focused plot on the higher end of the selectivity (>2) which has range 240K to 270K.

5.4 Preferential Adsorption Separation

PAS is performed with Co-MOF-74 for five different temperatures, the resulting selectivity is calculated. To fit these data, we explore the relation between selectivity and temperature. We model the separation process as a temperature-activated process, and by Arrhenius's equation, we expect:

$$\mathrm{S} = \mathrm{S}_0 e^{-E_a/(RT)}, \tag{5.1}$$

where S is the selectivity, S_0 is the pre-exponential factor (dimensionless in our case), E_a is the activation energy which should equal to the difference between the ZPEs of hydrogen and deuterium, R is the gas constant, and T is the temperature. Take the logarithm on both side of Eqn. 5.1, we obtain:

$$\ln(\mathrm{S}) = \ln(\mathrm{S}_0) - \frac{E_a}{RT} \tag{5.2}$$

Let $x = 1000/T$, and substitute x into Eqn. 5.2:

$$\ln(\mathrm{S}) = -\left(\frac{E_a}{1000R}\right)x + \ln(\mathrm{S}_0), \tag{5.3}$$

which is a linear relation between ln(S) and x.

Temperature (K)	Selectivity	x (1000/K)	ln(S)
50	7.55	20	2.02
60	5.22	16.7	1.65
75	3.34	13.3	1.21
100	2.12	10	0.75
120	1.66	8.33	0.51

Table 5.1: PAS results with Co-MOF-74

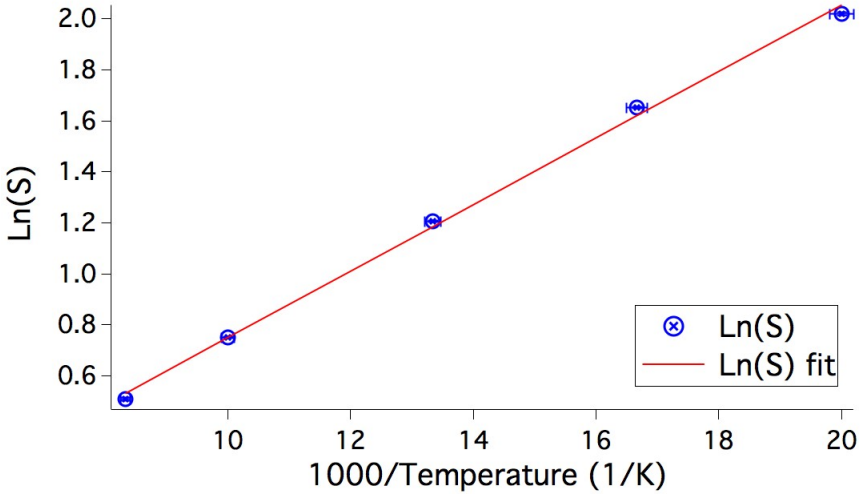

Figure 5.11: Experimental results and the fitting for PAS with Co-MOF-74

The fitting yields a value of $-E_a/(1000R)$=0.130K±0.002K and ln(S_0)=-0.557±0.050.

Table 5.1 sums T_{ads}, S, x, and ln(S) of the five PAS experiments and Fig. 5.11 shows the plotted data and the fit. The fitting yields a value for $-E_a/(1000R)$=0.130K±0.002K, which further yields a value for $-E_a$=1080J/mol±17J/mol. This is quite close (within 7 standard deviations) to the reported value of 0.97kJ/mol given the fact that this value of 0.97kJ/mol is determined with infrared spectra and a rough assumption of 3-D simple harmonic oscillator potential.[28]

Chapter 6

Conclusion and Future Work

6.1 Conclusion

In this thesis we present our research on hydrogen isotope separation using metal-organic frameworks (MOFs). We provide background on two state-of-art MOFs, Co-MOF-74 and Cu(I)-MFU-4l. Then we elaborate on the statistical theory of selectivity, the mechanism of separation and the basic idea of mass spectrometry. We provide a description of our experimental apparatus and procedures. TPD spectra, TPS results and PAS results are then presented.

Differences between two types of TPD spectra are discussed. We demonstrate that the pure-pure TPD spectra provides more direct information on the relation between ZPE and desorption temperatures whereas mixture TPD spectra can serve as predictions to direct TPS measurements.

Direct TPS measurements are also performed to confirm the TPD prediction. We conclude that TPD predictions are highly accurate within the some temperature range, although the exact cutoff still needs to be determined. With the TPD spectra, we predict a high selectivity of approximately 6 for TPS with Cu(I)-MFU-4l at a temperature of 263K. This shows the potential of Cu(I)-MFU-4l for hydrogen isotope separation.

Our values of the difference between the ZPEs of hydrogen and deuterium derived from PAS measurements coincide with the literature value which is based on infrared spectra and 3D simple harmonic oscillator potential.

6.2 Future Work

One obvious thing to do in the future is to repeat the TPS measurements with Cu(I)-MFU-4l. Direct measurements on the selectivity of Cu(I)-MFU-4l can help us confirm both the TPD prediction method and the separation ability of Cu(I)-MFU-4l. A more careful error analysis is necessary for determine the range of the TPD prediction.

PAS measurements on Cu(I)-MFU-4l is another thing to do. Infrared spectroscopy should also be carried out for Cu(I)-MFU-4l to repeat the calculation for the difference in translational zero point energy using 3D simple harmonic oscillator potential model. The results from these two measurements should be compared.

Appendix A

Hydrogen Isotope ZPE Visualizer

In this appendix, I attach my program which calculates and visualizes the zero point energy for hydrogen molecule and deuterium molecule in a user-defined one dimensional Lennard-Jones potential well.

The program is attached here in the form of a "modular package," which allows further modification if needed. For example Fig. 2.1 is generated from a modified version of this program.

Below is the code of the program (in Python 3):

```
##ZPEVisualizer_Package.py
##Modular package for hydrogen isotope zero point energy visualizer
##Naiyuan Zhang (James)
##I affirm that I have adhered to the Honor Code in this program.


####### REQUIRED IMPORT #######
###############################
```

```
import math
import numpy as np
import matplotlib.pyplot as plt
################################


##define basic variables
################################
mh=3674.305    #mass of H2 in natural units
md=7351.676    #mass of D2 in natural units
hbar=1
EL=0           ##zero point
SHOTEST=0      ##Test with simple harmonic oscillator? 1=Yes, 0=No
################################


##parameter input
################################
depth=eval(input("Please input the depth of the potential well in eV: "))
depth=depth/(2*13.6057) #switch to natural units
width=eval(input("Please input the width of the potential well in Ang: "))
width=width/1.8897 #switch to natural units
#ask for precision
n=input("Please give the number of grids for the matrices; hit 'retrun' to use default: ")
if n!="":
    n=eval(n)
else:
    n=2000
print("Would you like to enter the range of r? ")
rmin=input("Enter the minimum of r in Ang to continue; hit 'return' to skip: ")
if rmin!="":
    rmin=eval(rmin)
    rmax=eval(input("Please enter the maximum of r in Ang: "))
elif width>=10:
    rmin=width-5
    rmax=width+5
elif width>=3:
    rmin=1
    rmax=width*2+1
else:
    rmin=width/3
    rmax=width/3*5
################################


##define LJ potential
```

```
##############################
D=(rmax-rmin)/(n-1)
V=[]
for i in range (0, n):
    r=rmin+i*D
    V=V+[depth*((width/r)**12-2*(width/r)**6)]
##############################


##construct matrices
##############################
dh=[]    #main diagonal for h2
for i in range (0, n):
    dh=dh+[2+V[i]*2*D*D*mh/hbar/hbar]
Mh=np.zeros((n,n))     #construct the matrix for h2
for i in range (n):
    Mh[i][i]=dh[i]
for j in range(n-1):
    Mh[j][j+1]=-1
for k in range (1,n):
    Mh[k][k-1]=-1
MatrixH=np.matrix(Mh)

dd=[]    #main diagonal for d2
for i in range (0, n):
    dd=dd+[2+V[i]*2*D*D*md/hbar/hbar]
Md=np.zeros((n,n))     #construct the matrix for d2
for i in range (n):
    Md[i][i]=dd[i]
for j in range(n-1):
    Md[j][j+1]=-1
for k in range (1,n):
    Md[k][k-1]=-1
MatrixD=np.matrix(Md)
##############################


##diagonalize matrices
##############################
Ah,Bh=np.linalg.eigh(MatrixH)
Ad,Bd=np.linalg.eigh(MatrixD)
##############################


##reporting
##############################
```

```
GSEH=Ah[EL]/2/D/D/mh*hbar*hbar*(2*13.6057)    #ZPE for H2 in eV
GSED=Ad[EL]/2/D/D/md*hbar*hbar*(2*13.6057)    #ZPE for D2 in eV
print()
print("==========================================================================")
print("=================================REPORT===================================")
print("Depth and Width: ", -depth*(2*13.6057),"eV", width*1.8897,"Ang",sep='')
print("Number of grids: ", n)
print("Range of r: ",rmin*1.8897,"Ang",rmax*1.8897,"Ang", sep='')
print("Approximated Zero Point Energy for H2: ",GSEH,"eV",sep='')
print("Approximated Zero Point Energy for D2: ",GSED,"eV",sep='')
print("Difference between Zero Point Energies (Delta E): ", GSEH-GSED,"eV",sep='')
##############################


##construct the r-axis
##############################
raxis=[]
for i in range (0,n):
    raxis=raxis+[(rmin+i*D)*1.8897]
##############################


##construct the eigen energies
##############################
EigenEh=[] #prepare the dash lines for eigen energies of h2
EigenEd=[] #prepare the dash lines for eigen energies of d2
for i in range(0,n):
    EigenEh=EigenEh+[GSEH]
    EigenEd=EigenEd+[GSED]
##############################


##construct the potential well
##############################
well=[]
for i in range(0,n):
    well=well+[(V[i]*(2*13.6057))]
##############################


##construct the wavefunction for h2, ensure the peak is upward
##############################
testh=(Bh[:,EL]).getA()
MAXh=np.amax(testh)
MINh=np.amin(testh)
Maxh=abs(MAXh)
```

```
Minh=abs(MINh)
if Maxh>Minh:
    Rh=Maxh/Minh     #define "peak ratio" for h2
    factor=1
else:
    Rh=Minh/Maxh     #define "peak ratio" for h2
    factor=-1
ylistH=[]    #prepare H2 wavefunction for plotting
for i in Bh[:,EL]:
    k=i[0,0]
    ylistH=ylistH+[factor*k+GSEH]
wavefnH=np.array(ylistH)
################################


##construct the wavefunction for d2, ensure the peak is upward
################################
testd=(Bd[:,0]).getA()
MAXd=np.amax(testd)
MINd=np.amin(testd)
Maxd=abs(MAXd)
Mind=abs(MINd)
if Maxd>Mind:
    Rd=Maxd/Mind     #define "peak ratio" for d2
    factor=1
else:
    Rd=Mind/Maxd     #define "peak ratio" for d2
    factor=-1
ylistD=[]    #prepare the wavefunction for H2
for i in Bd[:,EL]:
    k=i[0,0]
    ylistD=ylistD+[factor*k+GSED]
wavefnD=np.array(ylistD)
################################


##Peak Ratio Test
################################
if Rh>Rd:     #use the small peak ratio to test
    R=Rd
else:
    R=Rh
if R>1000:
    print("Peak ratio test passed. ")
else:
    print("Peak ratio low. Measure of Precision: R=", R)
```

```
print("=============================================================================")
##
##By using the matrices, we actually assume that the first point
##    of the wave function is small enough to be treated as zero.
##Peak ratio test compares the the peak of the wave function
##                        and the first point of the wave function.
##If this ratio is greater than 1000, we assume that our
##                                      assumption is precise enough.
## else we print out the ratio to provide some information on
##                      the degree of precision of this assumption.
###############################




##Simple Harmonic Oscillator Test
###############################
##Use SHO to approximate the result
##Since we can analytically solve SHO
##this approximation provides a test to see
##whether the program is giving physical results
##
SHOTEST=1 #1=test provided, 0=test not provided
k=72*depth/width/width     ##equaling 2nd derivatives
Vsho=[] #constructing the sho potential
for i in range (0,n):
    r=rmin+i*D
    Vsho=Vsho+[(0.5*k*(r-width)**2-depth)*(2*13.6057)]

omegaH=(k/mh)**0.5 #Exact solutions for SHO
omegaD=(k/md)**0.5
GSshoH=((EL+0.5)*hbar*omegaH-depth)*(2*13.6057)
GSshoD=((EL+0.5)*hbar*omegaD-depth)*(2*13.6057)

EshoH=[]
EshoD=[]
for i in range (0,n):
    EshoH=EshoH+[GSshoH]
    EshoD=EshoD+[GSshoD]
print()
print("=============================================================================")
print("=================================SHO Test====================================")
print("SHO Test included.")
print("Zero Point Energy for H2 from SHO Test: ",GSshoH,"eV",sep='')  #report the solutions
print("Zero Point Energy for D2 from SHO Test: ",GSshoD,"eV",sep='')
```

```
print("Difference between Zero Point Energies from SHO Test: ", GSshoH-GSshoD,"eV",sep='')
print()
print("Differnece between LJ and SHO for H2: ", GSEH-GSshoH,"eV",sep='') #report the test
print("Differnece between LJ and SHO for D2: ", GSED-GSshoD,"eV",sep='')
print("Difference between LJ and SHO for delta E: ", (GSEH-GSED)-(GSshoH-GSshoD),"eV",sep='')
print("Percentage of difference for delta E: ",
      abs((GSEH-GSED)-(GSshoH-GSshoD))/(GSEH-GSED)*100,"%",sep='')
print("=============================================================================")
##############################
```

```
##plotting & quitting
##############################
print()
print("=============================================================================")
print("==============================Plotting=======================================")
print("Plotting the Wave Functions now. ")
print("H2: Blue")
print("D2: Red")

#Plot without SHO Test
if SHOTEST==0:
    plt.plot(raxis,EigenEh,"b--", raxis, EigenEd, "r--",
             raxis, wavefnH,"b-",raxis, wavefnD,"r-",raxis,well,"k")
    plt.title("Plot of the Wave Function")
    plt.xlabel("r")
    plt.ylabel("Energy (eV)")
    plt.xlim(rmin*1.8897,rmax*1.8897)
    plt.ylim(-depth*1.2*(2*13.6057),depth*0.2*(2*13.6057))
    plt.grid(True)
    print("Close the graph tab to quit.")
    print("=============================================================================")
    plt.show()

#Plot without SHO Test
elif SHOTEST==1:
    print("Lennard-Jones: Solid lines")
    print("SHO Approximation: Dashed lines")
    plt.plot(raxis,EigenEh,"b-",raxis, EigenEd,"r-",
             raxis,wavefnH,"b-",raxis,wavefnD,"r-",
             raxis,well,"k",raxis,Vsho,"k--",
             raxis,EshoH,"b--",raxis,EshoD,"r--")
    plt.title("Plot of the Wave Function")
```

```
    plt.xlabel("r (Ang)")
    plt.ylabel("Energy (eV)")
    plt.xlim(rmin*1.8897,rmax*1.8897)
    plt.ylim(-depth*1.2*(2*13.6057),depth*0.2*(2*13.6057))
    plt.grid(True)
    print("Close the graphic tab to quit.")
    print("================================================================================")
    plt.show()
quit()
##############################
```

Appendix B

PAS Pressure Correction

Here we present a more detailed explanation on the pressure correction for selectivity calculation for PAS. First we define the following numbers:

P1=the pressure of the portion above the sample valve,

P2=the pressure of the the portion below the sample valve,

R1=the ratio of the amount of H_2 in the portion above,

R2=the ratio of the amount of H_2 in the portion below,

V1=the volume above,

V2=the volume below,

T=the temperature at which this PAS is performed (T_{ads}),

Tf=the final temperature V2 is heated to,

where P1 and P2 are measured by the pressure gauge in ASAP 2020 and recorded by LabView program, R1 and R2 are calculated from the measurement by mass spectrometer, V1 and V2 are

given by the design of the system, T and Tf are given as parameters of the experiment.

Before we evacuate the portion above, the system is at equilibrium and hence P1 is true for both V1 and V2. Use the ideal gas law, we can find the total amount of gas of the residue:

$$n_{\mathrm{r}} = n_{\mathrm{r,a}} + n_{\mathrm{r,b}} = \frac{\mathrm{P1} \cdot \mathrm{V1}}{R\mathrm{T}_{\mathrm{room}}} + \frac{\mathrm{P1} \cdot \mathrm{V2}}{R\mathrm{T}}, \tag{B.1}$$

where n_{r} is the amount of molecules of the residue, $n_{\mathrm{r,a}}$ is the amount of molecules of the above portion of the residue, $n_{\mathrm{r,b}}$ is the amount of molecules of the below portion of the residue, R is the gas constant, and $\mathrm{T}_{\mathrm{room}}$ is the room temperature (298K).

Again by ideal gas law, we can also find the total amount of gas of the product:

$$n_{\mathrm{p}} = n_{\mathrm{b}} - n_{\mathrm{r,b}} = \left(\frac{\mathrm{P2} \cdot \mathrm{V1}}{R\mathrm{T}_{\mathrm{room}}} + \frac{\mathrm{P2} \cdot \mathrm{V2}}{R\mathrm{Tf}} \right) - \frac{\mathrm{P1} \cdot \mathrm{V2}}{R\mathrm{T}}, \tag{B.2}$$

where n_{p} is the amount of molecules of the product, n_{b} is the amount of molecules of the below portion, $n_{\mathrm{r,b}}$ is the amount of molecules of the below portion of the residue.

Then with R1 and R2, we find the number of hydrogen in each portion to be:

$$n_{\mathrm{H,r}} = \mathrm{R1} \cdot n_{\mathrm{r}} = \mathrm{R1} \cdot (n_{\mathrm{r,a}} + n_{\mathrm{r,b}}), \tag{B.3}$$

$$n_{\mathrm{H,p}} = n_{\mathrm{H,b}} - n_{\mathrm{H,r,b}} = \mathrm{R2} \cdot n_{\mathrm{b}} - \mathrm{R1} \cdot n_{\mathrm{r,b}}, \tag{B.4}$$

and the number of hydrogen in each portion to be:

$$n_{\mathrm{D,r}} = (1 - \mathrm{R1}) \cdot n_{\mathrm{r}} = (1 - \mathrm{R1}) \cdot (n_{\mathrm{r,a}} + n_{\mathrm{r,b}}), \tag{B.5}$$

$$n_{\mathrm{D,p}} = n_{\mathrm{D,b}} - n_{\mathrm{D,r,b}} = (1 - \mathrm{R2}) \cdot n_{\mathrm{b}} - (1 - \mathrm{R1}) \cdot n_{\mathrm{r,b}}. \tag{B.6}$$

With these values, the selectivity is straightforwardly:

$$\mathrm{S} = \frac{n_{\mathrm{D,p}}/n_{\mathrm{H,p}}}{n_{\mathrm{D,r}}/n_{\mathrm{H,r}}} \tag{B.7}$$

Bibliography

[1] G. M. Hornberger. New manuscript guidelines for the reporting of stable hydrogen, carbon, and oxygen isotope radio data. *Water Resources Research*, 31:2895–2896, 1995.

[2] Catherine E. Housecroft and Alan G. Sharpe. *Inorganic Chemistry*. Pearson, 2th edition edition, 2005.

[3] Charles Schmidt. First deuterated drug approved. *Nature Biotechnology*, 35(6):493, Jun 1, 2017.

[4] Scott L. Harbeson and Roger D. Tung. *Deuterium in Drug Discovery and Development*, volume 46 of *Annual Reports in Medicinal Chemistry*, pages 403–417. Elsevier Science Technology, 2011.

[5] Chris Waltham. An early history of heavy water. Jun 20, 2002.

[6] Nathan Lifson, George B. Gordon, and Ruth McClintock. Measurement of total carbon dioxide production by means of d2o181. *Obesity Research*, 5(1):78–84, Jan 1997.

[7] Joseph P. Hornak. The Basics of NMR. http://www.cis.rit.edu/htbooks/nmr/inside.htm, 1997.

[8] Alistair I. Miller. Heavy Water: A Manufacturers' Guide for the Hydrogen Century. https://cns-snc.ca/media/Bulletin/A_Miller_Heavy_Water.pdf, 2001.

[9] Jian-Rong Li, Ryan J. Kuppler, and Hong-Cai Zhou. Selective gas adsorption and separation in metal-organic frameworks. *Chemical Society reviews*, 38(5):1477, May 2009.

[10] Jesse L. C. Rowsell and Omar M. Yaghi. Metal–organic frameworks: a new class of porous materials, 2004.

[11] Hyunchul Oh, Ievgeniia Savchenko, Andreas Mavrandonakis, Thomas Heine, and Michael Hirscher. Highly effective hydrogen isotope separation in nanoporous metal-organic frameworks with open metal sites: direct measurement and theoretical analysis. *ACS nano*, 8(1):761, Jan 28, 2014.

[12] Stuart R. Batten, Neil R. Champness, Xiao-Ming Chen, Javier Garcia-Martinez, Susumu Kitagawa, Lars Öhrström, Michael O'Keeffe, Myunghyun Paik Suh, and Jan Reedijk. Terminology of metal–organic frameworks and coordination polymers (iupac recommendations 2013). *Pure and Applied Chemistry*, 85(8):1715–1724, Jul 31, 2013.

[13] Yun Liu, Houria Kabbour, Craig M. Brown, Dan A. Neumann, and Channing C. Ahn. Increasing the density of adsorbed hydrogen with coordinatively unsaturated metal centers in metal-organic frameworks. *Langmuir : the ACS journal of surfaces and colloids*, 24(9):4772–4777, May 6, 2008.

[14] Leslie J. Murray, Mircea Dincă, and Jeffrey R. Long. Hydrogen storage in metal-organic frameworks. *Chemical Society reviews*, 38(5):1294, May 2009.

[15] Kai Shinbrough. Honors Thesis: Infrared and Thermal-Desorption Spectroscopy of H2 and D2

in Metal Organic Frameworks. Physics and Astronomy Department, Oberlin College, March 2017.

[16] Matthew T. Kapelewski, Stephen J. Geier, Matthew R. Hudson, David Stück, Jarad A. Mason, Jocienne N. Nelson, Dianne J. Xiao, Zeric Hulvey, Elizabeth Gilmour, Stephen A. FitzGerald, Martin Head-Gordon, Craig M. Brown, and Jeffrey R. Long. M2(m-dobdc) (m = mg, mn, fe, co, ni) metal-organic frameworks exhibiting increased charge density and enhanced h2 binding at the open metal sites. *Journal of the American Chemical Society*, 136(34):12119, Aug 27, 2014.

[17] I Weinrauch, I Savchenko, D Denysenko, S M Souliou, H h Kim, M Le Tacon, L L Daemen, Y Cheng, A Mavrandonakis, A J Ramirez-cuesta, D Volkmer, G Schütz, M Hirscher, and T Heine. Capture of heavy hydrogen isotopes in a metal-organic framework with active cu(i) sites. *Nature Communications*, 8:14496, Mar 1, 2017.

[18] Dmytro Denysenko, Maciej Grzywa, Jelena Jelic, Karsten Reuter, and Dirk Volkmer. Scorpionate-type coordination in mfu-4l metal–organic frameworks: Small-molecule binding and activation upon the thermally activated formation of open metal sites. *Angewandte Chemie International Edition*, 53(23):5832–5836, Jun 2, 2014.

[19] Ian D. Wilson. *Encyclopedia of separation science*. Academic Press, San Diego [u.a.], 2000.

[20] Tom Fawcett. An introduction to roc analysis. *Pattern Recognition Letters*, 27(8):861–874, 2006.

[21] Afina S. Glas, Jeroen G. Lijmer, Martin H. Prins, Gouke J. Bonsel, and Patrick M. M. Bossuyt. The diagnostic odds ratio: a single indicator of test performance. *Journal of Clinical Epidemiology*, 56(11):1129–1135, 2003.

[22] Qinyu Wang, Sivakumar R. Challa, David S. Sholl, and J. Karl Johnson. Quantum sieving in carbon nanotubes and zeolites. *Physical Review Letters*, 82(5):956–959, Feb 1999.

[23] Hiden Analytical. Relative Sensitivity, RS Measurements of Gases. Gas Analysis, Application Note 282.

[24] R. Davis, M. Frearson, and M. E. Rose. Mass spectrometry — analytical chemistry by open learning (acol). *Analytica Chimica Acta*, 219:358–359, 1989.

[25] Youmei Peng, Tiefeng Cheng, Lihong Dong, Yuhai Zhang, Xiaojing Chen, Jinhua Jiang, Jingmin Zhang, Xiaohe Guo, Mintong Guo, Junbiao Chang, and Qingduan Wang. Quantification of 2'-deoxy-2'--fluoro-4'-azidocytidine in rat and dog plasma using liquid chromatography-quadrupole time-of-flight and liquid chromatography-triple quadrupole mass spectrometry: Application to bioavailability and pharmacokinetic studies. *Journal of pharmaceutical and biomedical analysis*, 98:379–386, Sep 2014.

[26] James S. Allen. An improved electron multiplier particle counter. *Review of Scientific Instruments*, 18(10):739–749, Oct 1947.

[27] Eric Stauffer, Julia Ann Dolan, and Reta Newman. Fire debris analysis, 2008.

[28] Stephen A. FitzGerald, Christopher J. Pierce, Jesse L. C. Rowsell, Eric D. Bloch, and Jarad A. Mason. Highly selective quantum sieving of d2 from h2 by a metal-organic framework as determined by gas manometry and infrared spectroscopy. *Journal of the American Chemical Society*, 135(25):9458, Jun 26, 2013.